VELOCITY-SPACE RING-PLASMA INSTABILITY MAGNETIZED

PART II: SIMULATION

by

J.K. Lee and C.K. Birdsall

Memorandum No. UCB/ERL M78/39

28 June 1978

ELECTRONICS RESEARCH LABORATORY

College of Engineering
University of California, Berkeley
94720

TABLE of CONTENTS

ABSTRACT

The ring-plasma instability arising due to two-energy component ions of a homogeneous plasma in a uniform magnetic field is studied through use of electrostatic and electromagnetic simulations, treating the ring ions as particles and the target plasma (ions and electrons) as linearized fluids. Simulation results verify very closely the predictions of the linear Vlasov theory (presented in Part 1) and provide extensive information on nonlinear features such as beam spreading, slowing down, and saturation, some of which are in agreement with analytic explanations. This nonlinear evolution occurs before Coulomb collisions take place, and may be considered as initial conditions for Fokker-Planck calculations. The justification of using a linearized fluid is also discussed.

I. INTRODUCTION

The ring-plasma instability is studied through computer simulations, complementing the results of the linear Vlasov theory presented in the preceding paper, Part I.

The first simulation for this instability was that of Birdsall and Maron (1976) using a particle code. Their simulations had large noise due to the particles in the dense plasma component which almost obscured the instability itself, thus providing only a qualitative verification of the instability.

On the suggestion of A. B. Langdon, we constructed a hybrid code combining a particle code for the ring particles and, to reduce the dense plasma noise, a linearized Eulerian fluid for the plasma component. The result was as desired, almost noiseless. These hybrid codes (two versions: electrostatic and electromagnetic) have been used successfully to study the ring-plasma instability in the three density regimes presented earlier in Part I.

The agreement between the simulations and the results of the linear Vlasov theory is almost exact in all three regimes both for electrostatic and for electromagnetic cases.

In addition to the small amplitude behavior, hybrid simulations provide useful information on some nonlinear phenomena. The nonlinear evolution observed in simulations shows an appreciable average slowing and broadening of the ring in $v_\perp$ space in a short time, on the order of an ion cyclotron period, at about the time the growing field energy reaches its first peak value (called the saturation in this

paper). The slowing and spreading are not due to collisions. Considerable structure has been observed in the velocity-space $v_\perp$ perpendicular to the magnetic field; in some examples, there are radial limits imposed by the zeroes of Bessel functions, and with the average $v_\perp$ at saturation corresponding closely to the first peak of Bessel functions (so far this has been checked mainly for the weak ring regime). The rapid slowing and spreading of the ring, which occur much before collisions take place, should be taken into account in fusion reactor neutral beam injection studies, especially in the reactivity calculations, which usually assume a monoenergetic beam and do not consider this "initial" slowing and spreading.

The electrostatic two ion species simulations model, using the particle-fluid hybrid code, is presented in Sec. II. The comparison of simulation with the results of the linear theory is presented in Sec. III. Nonlinear evolution such as beam spreading, average slowing down, and saturation are discussed in Sec. IV. Next, typical results of electromagnetic simulations are shown in Sec. V. A discussion on the limits of the linearity assumption for the fluid plasma is given in Sec. VI. Section VII discusses which Bernstein harmonics (i.e., those of the ring or of the plasma) are involved when the lower hybrid wave coupling occurs (in the weak ring case), using the comparison of fluid-particle simulations with wholly particle theory. Conclusions are provided in Sec. VIII.

II. MODEL for ELECTROSTATIC HYBRID SIMULATION

A particle-only code has been used to simulate a ring-plasma instability with limited success; the difficulty was that the noise from the dense warm plasma component tended to obscure the instability itself. The results of a particle code [Birdsall *et al.* (1976)] using one spatial and two velocity dimensions (1d2v) are shown as a comparison in Fig. 1.

A way of reducing this noise as well as the computing cost was suggested by A. B. Langdon (at Lawrence Livermore Laboratory); this is to treat the warm plasma as a linearized Eulerian fluid rather than as particles. The fluid equations are the Lorentz equation of motion with a scalar pressure, no collisions, with equation of continuity, and the adiabatic equation of state (ratio of specific heats is 3).

This scheme has an additional advantage that with the plasma variables known only on the spatial grid (i.e., the plasma dynamics produces no aliases), there is no (alias caused) limit on the smallness of the parameter $\lambda_D/\Delta x$ (where λ_D is the Debye length and Δx is the spatial grid size) as in a particle code. The computing cost is also greatly reduced by replacing the dense plasma particles by an Eulerian fluid. There is a penalty in that the fluid part is linear, so that fluid is limited to small perturbations; the ring, of course, is composed of particles and may become highly nonlinear.

The hybrid code (ES1 + EFL) is constructed by combining a particle code (ES1 by A. B. Langdon) for the fully nonlinear ring with a linearized Eulerian fluid code (EFL) for the warm plasma. The detailed algorithm for this 1d2v code will appear elsewhere [Lee and Birdsall (1978)].

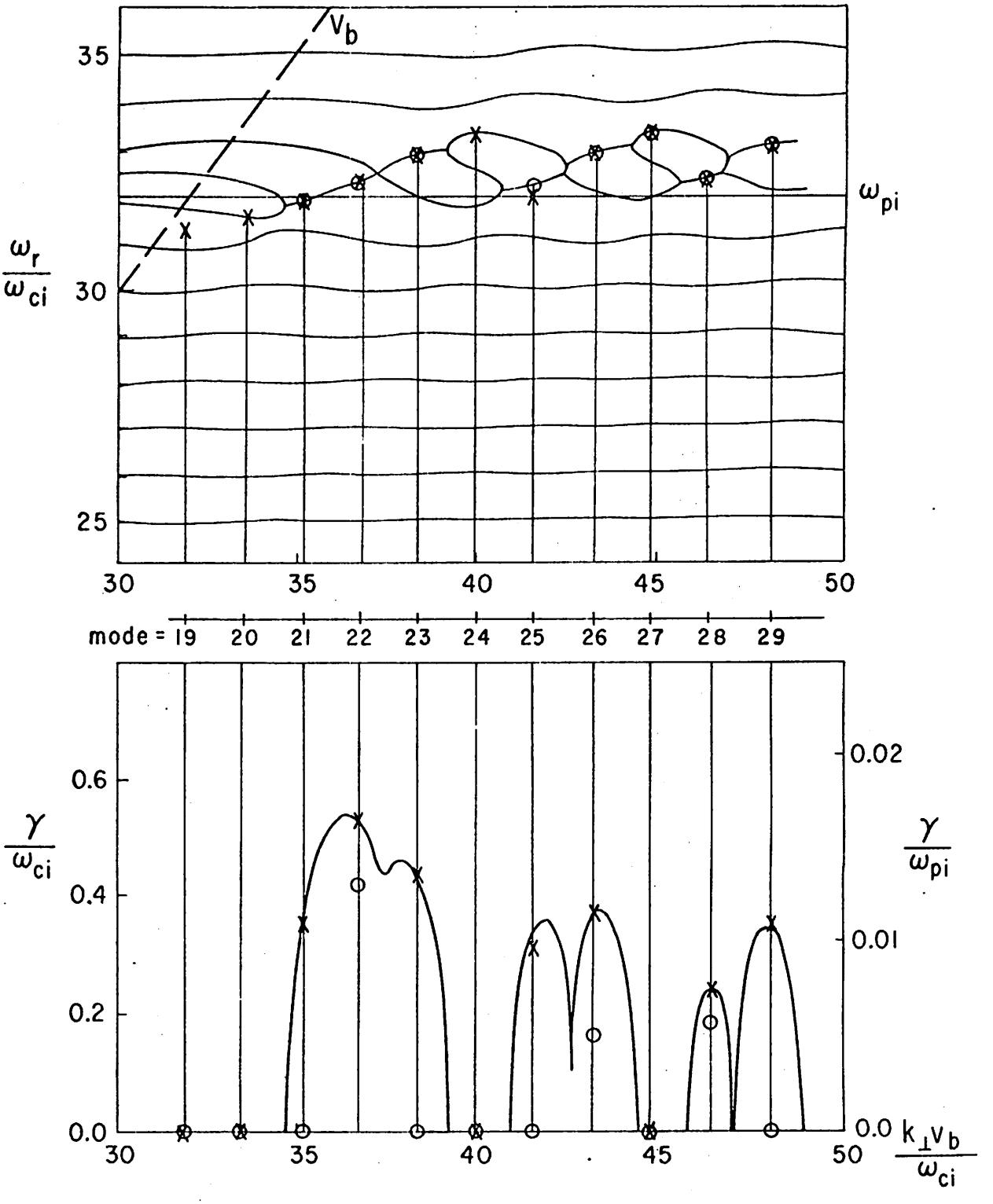

Fig. 1 Electrostatic dispersion curves for $R = 10^{-3}$, $\omega_{ppi}/\omega_{ci} \approx 32$, $v_b/v_{tp} \approx 13$ with no electron dynamics; continuous curves are the results of the theory compared with the particle code results [Birdsall et al., (1976)] (marked as 0) and the hybrid code results (marked as x). Note that there is no growth at smaller k (i.e., at $k_\perp v_b/\omega_{ci} \lesssim 30$).

III. VERIFICATION of LINEAR THEORY, ELECTROSTATIC

The small amplitude frequencies and the growth rates for the ring-plasma electrostatic instability, found using the code, ROOTS [Gerver (1976)], are compared with the electrostatic simulation results of both the hybrid code [Lee and Birdsall (1977)] and the particle code [Birdsall *et al.* (1976)] in Fig. 1 as a sample verification. The physical parameters for the simulation are the same as the prototype in the theory (see the previous paper, Part I); the numerical parameters are:

$$NP = 8192$$

$$NG \equiv L/\Delta x = 256$$

$$\omega_{ppi}\Delta t \simeq 0.32$$

$$\lambda_D/\Delta x = 0.322$$

$$L/\lambda_D = 82.4$$

$$k_\perp \lambda_D = 0.16 \quad \text{(at mode 20)}$$

where NP and NG are the numbers of particles and spatial grids, respectively, L is the simulation length, Δx is the spatial grid size, Δt is the time step, and λ_D is the Debye length of plasma ions. Compared with the qualitative verification of the existence of the instability by the wholly particle code, the hybrid results check remarkably well with the linear theory. This latter agreement of the hybrid code with theory extends to most of the simulation runs, for several cases in each regime, from $R = 5 \times 10^{-4}$ to 1.0; these are not shown in this paper. Thus, most of the theoretical results in Part I are verified by the

hybrid simulations. The theoretical results will be used interchangeably with the simulation results in the following sections.

IV. NONLINEAR EVOLUTION; CHECK with SOME ANALYTIC PREDICTIONS

As a result of this instability, the initial cold ring distribution spreads out in the velocity-space ($v_\perp$) perpendicular to the magnetic field and decreases its average perpendicular speed in a time scale on the order of an ion cyclotron period as can be seen in Fig. 2. The spreading and slowing down of the beam are not due to Coulomb collisions because this time scale is much faster than the usual collision-caused Fokker-Planck times (either drag or diffusion times) for typical fusion parameters.

In the following we identify the radial and the angular boundaries in $v_\perp$-space of spread beam particles in terms of the properties of an analytic function for a specific case, namely, $R = 10^{-2}$, $\omega_{ppi}/\omega_{ci} = 10$, $v_b/v_{tp} \tilde{\approx} 13$. The dispersion curves for these parameters are shown in Fig. 3, where we observe that the coupling between the lower hybrid wave and the tenth Bernstein harmonic of beam ions provides the most unstable mode. This instability mechanism is similar to that of the weak ring regime discussed in Part I although the ring density classifies this case to the intermediate regime; this discrepancy is due to the choice of a nonprototype parameter for ω_{ppi}/ω_{ci}, namely, 10 here instead of 32 as before.

Following the Hamiltonian approach [Timofeev (1974), Fukuyama *et al.* (1977)], the equation of motion for the conjugate momentum is

$$\frac{dk_\perp a_{ib}}{dt} \propto J_\ell(k_\perp a_{ib}) \qquad \text{where} \quad a_{ib} \equiv \frac{v_b}{\omega_{ci}} \qquad (1)$$

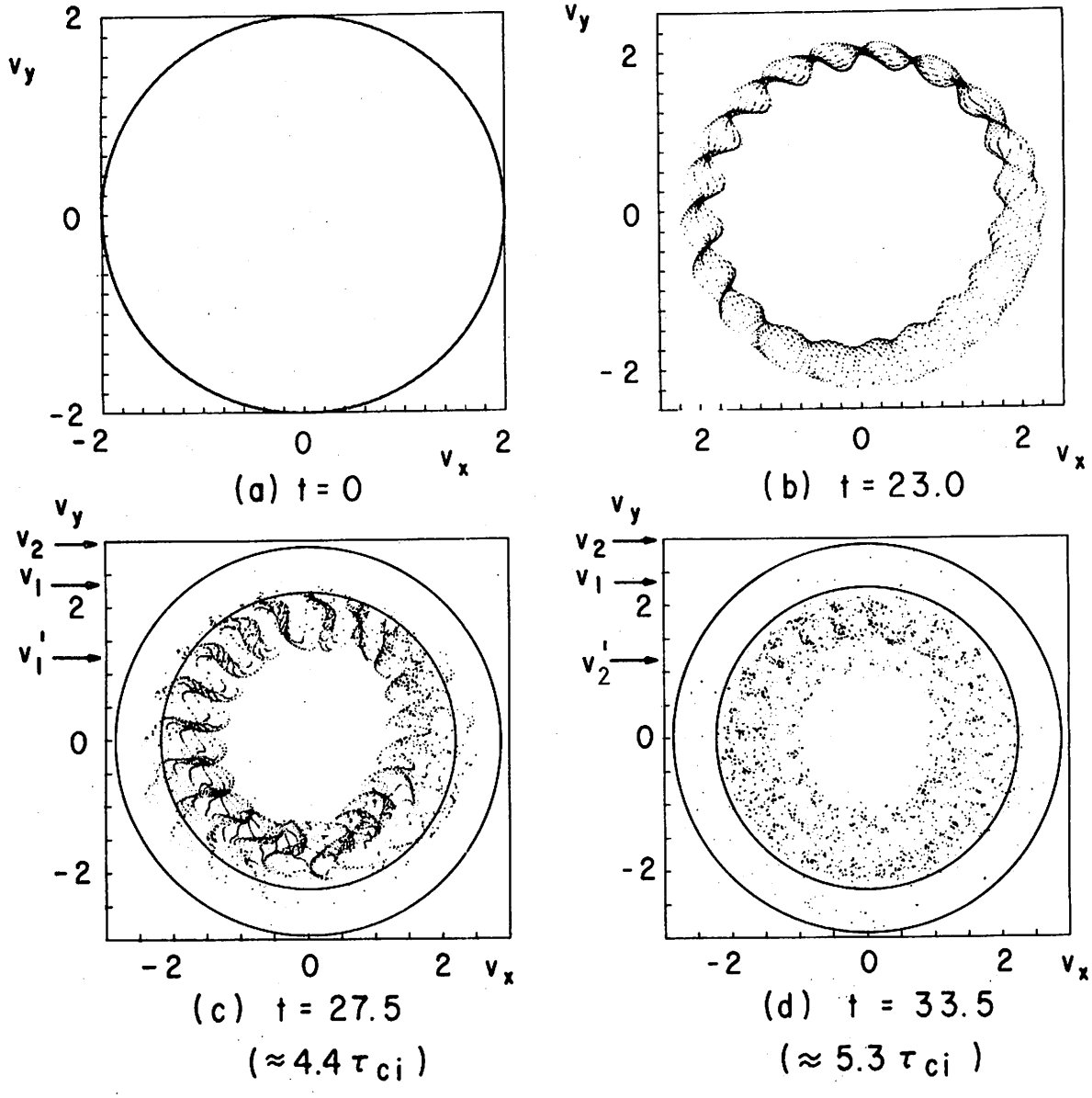

Fig. 2 The time evolution of a ring distribution in $v_x - v_y$ space with $\underline{k} = k_x \hat{x}$ and $\underline{B} = B_o \hat{z}$. Due to the interaction with the target plasma at the center (not drawn here), the ring particles spread outward and inward, and decrease their mean perpendicular speed. At about the saturation time ($t \approx 4.4\tau_{ci}$, where $\tau_{ci} = 2\pi/\omega_{ci} = 2\pi$), most ring particles are seen to be confined in a radial cell with outer boundary v_1 and inner boundary v_1' (note that the initial speed was $v_b = 2.0$); later after the saturation ring particles are seen to form two distinct cells. The two circles in Figs. (c) and (d) were drawn as best indicating these boundaries and not from analysis.

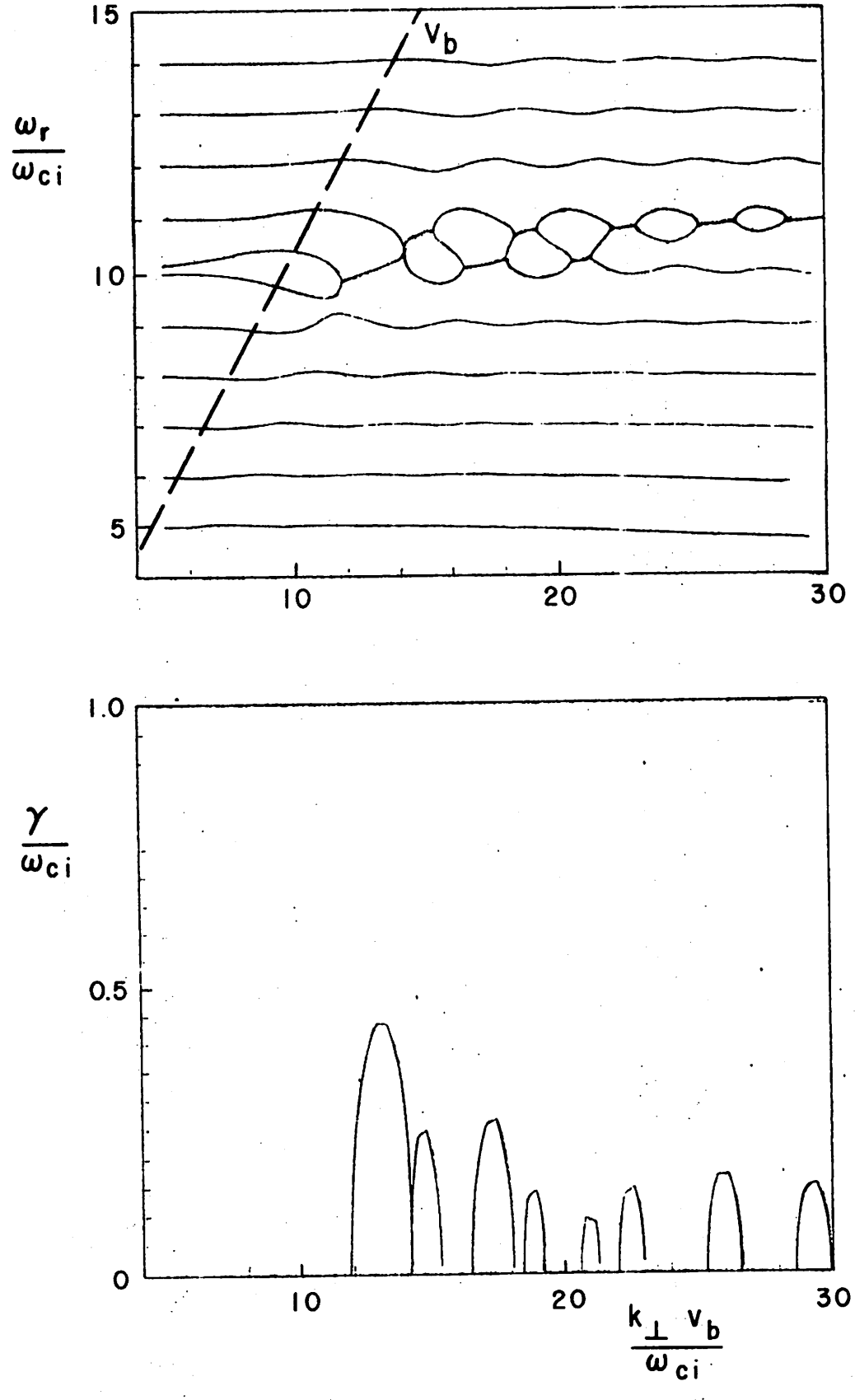

Fig. 3 Electrostatic dispersion curves for $R = 10^{-2}$, $\omega_{ppi}/\omega_{ci} = 10$, $v_b/v_{tp} \approx 13$ with no electron dynamics.

Thus, the motion of ring particles is closely related to the corresponding Bessel function of order ℓ, $J_\ell(k_\perp a_{ib})$. We will use this approach to explain the boundaries in $v_\perp$ space of the spread beam particles in the next section.

(1) *Spreading of Beam Particles*

In Figs. 2b,c,d, we observe that beam particles appear to be distorted into ten sinusoids around the ring, which we take as a manifestation of the major interaction being that of the tenth Bernstein harmonic and the lower hybrid wave, as also seen in Fig. 3. The Bessel index ℓ is 10 for this case. This identification was made earlier by Aamodt and Bodner (1969).

Figure 2c, which represents the $v_\perp$ - distributions at about the saturation time, shows distinct radial boundaries, inner (v_1') and outer (v_1). Figures 2d and 4 show the distribution at a time much later than the wave saturation, now with changed radial outer boundary (v_2) and inner boundary (v_2').

By analogy with the nonlinear theory of Aamodt (1970) and Aamodt and Bodner (1969), for a flute-like mode, we can view the spreading and the slowing in the following way.

The large difference in initial velocity distributions of ring and plasma provides the free energy source to drive an instability. As the instability develops, the initial ring will spread out in the $v_\perp$-space, both outward and inward, and at the same time its average speed will decrease. Up to the saturation time, most particles are confined in the first cell whose outer edge is determined by the first zero of the Bessel function of the tenth order $J_{10}(k_\perp a_{ib})$. After saturation some particles will leak out of the first cell to fill up the neighboring second cell, whose outer boundary is the second zero of $J_{10}(k_\perp a_{ib})$, until the distributions in both cells become flattened

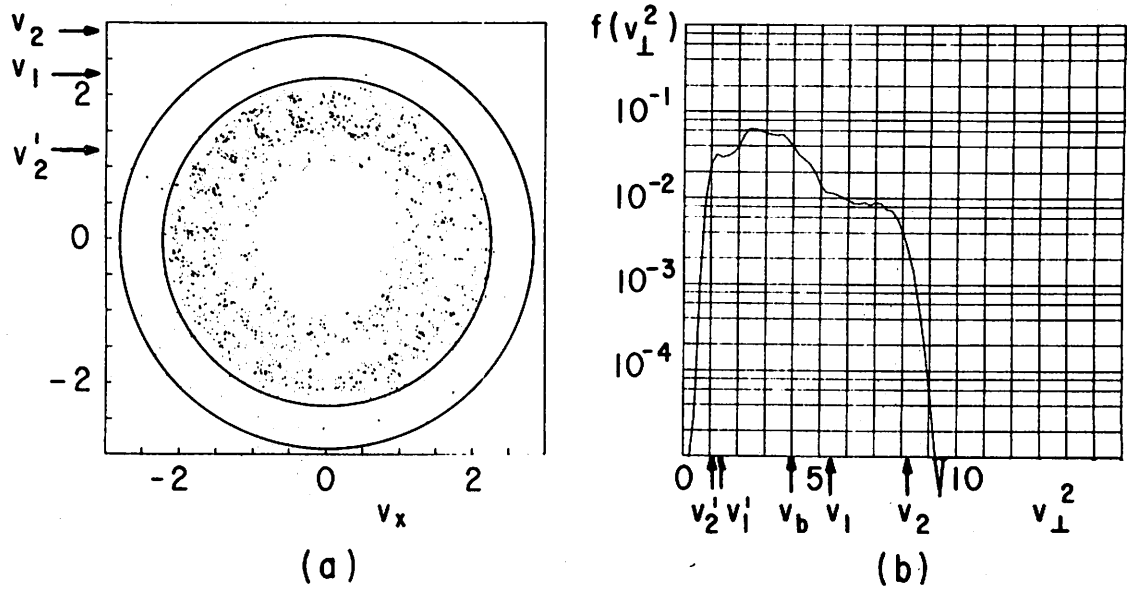

Fig. 4 (a) The snapshot at $t = 33.5$, much later than the saturation time identical to Fig. 2d.

(b) The corresponding velocity distribution function. Note that $v_b=2$ is the initial ring perpendicular speed and that v_1 and v_1' are the outer and inner boundaries of the first confining cell (corresponding to the saturation time, $t = 27.5$), while v_2 and v_2' are those of the second cell formed by the further spreading at $t = 33.5$.

(see Fig. 4b). The observed outer boundaries agree very well with the values predicted by the Bessel zeros. For example, for the first cell, Fig. 2c gives the simulation first outer boundary $v = 2.27$ which is identical to the first zero of $J_{10}(k_\perp a_{ib})$ shown in Fig. 5a. For the second cell v_2 (simulation) $= 2.88$, which is just the second zero of J_{10} in Fig. 5.

Like Aamodt (1970), we may use the effective potential energy of ring particles in the perpendicularly propagating wave to explain the inner boundaries. When we have a single resonance, the effective potential energy (see Fig. 5b) at the first outer boundary (v_1) will be zero; thus, particles have only the first cell to fill up and its inner boundary will be essentially zero. But, as in the present case, most ring-plasma instabilities have more than one gyroresonances as seen in dispersion curves (see Fig. 3). This reduces the effective potential energy at v_1 from zero to some finite lower value. As a result some particles leak out of the first cell until they form a somewhat flattened distribution in the second cell. The inner boundary (v_1') of the first cell corresponds to the same effective potential energy as that at the outer boundary (v_1) as in the usual trapping argument. Likewise v_2' corresponds to v_2 with the same effective potential energy. As time goes on, the inner boundary moves toward the inside due to the slight rise in the effective potential energy at v_2 compared to v_1. Simulation shows that inner boundaries are moving inward slowly (due to the slowly varying effective potential energy near the origin).

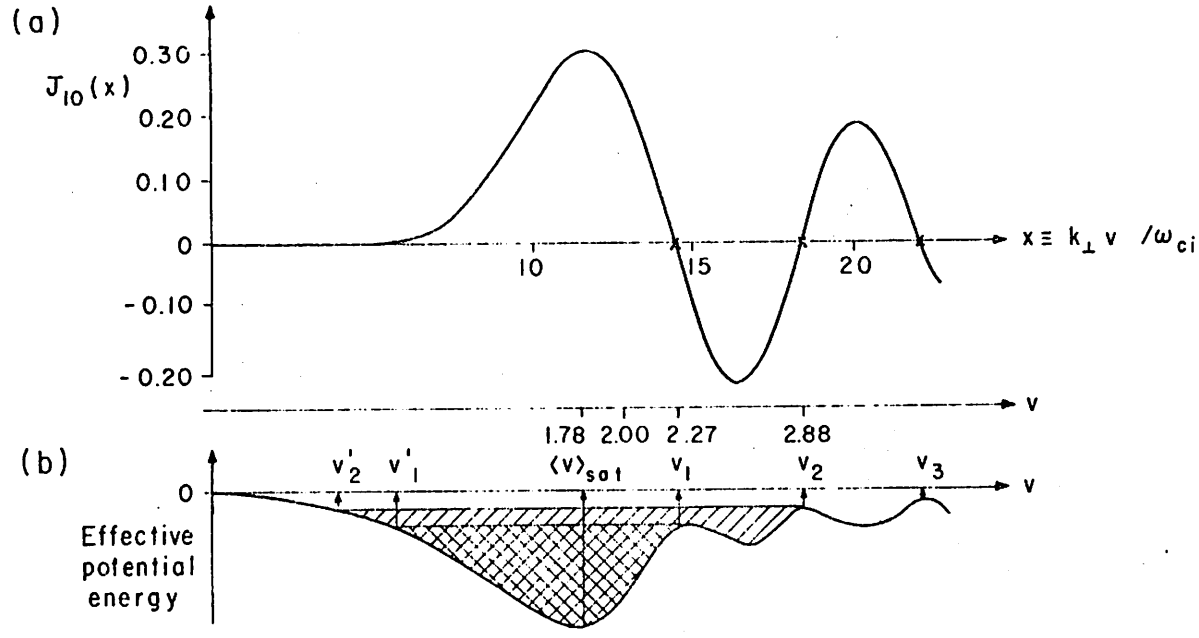

Fig. 5 (a) Bessel function of the first kind of order 10; $x = 14.5$ corresponds to $v = 2.27$, etc.

(b) The effective potential energy (postulated) of ring particles in the presence of a perpendicularly propagating wave; v_i refers to the outer-boundary of the i^{th} cell, v_i' to its inner boundary, and $\langle v \rangle_{sat}$ is the average beam speed at the saturation corresponding to the maximum of $J_{10}(x)$.

Figures 2c,d, show $v_2' \approx 1.05 < v_1' \approx 1.20$. Although this latter argument concerning the inner boundaries is only a qualitative one compared to the quantitative one for the outer boundaries, these simulation results could be regarded as a confirmation of the analytic theory of Aamodt and Bodner (1969).

(2) SLOWING DOWN OF BEAM PARTICLES

Figure 6 shows how ring particles are slowed down on the average due to the instability. As the wave grows to large amplitude, the average beam speed drops rapidly to reach the first minimum ($\langle v \rangle_{sat}$ in Fig. 6) and then rises and oscillates as in the more familiar trapped particle saturation in a beam-plasma instability; the last phenomenon, oscillation, is not shown in Fig. 6, but is clearly observed in the intermediate or strong beam cases. The failure to regain the original speed, $v_b = 2.0$ in Fig. 6 is taken to be similar to phase mixing in the beam-plasma mode.

From the Bessel function graph (Fig. 5a) we expect that the wave grows until the argument, $k_\perp v_b/\omega_{ci}$, of the Bessel function makes the Bessel function take the peak value, i.e., for our case $\langle v \rangle_{sat} = 1.78$ is expected from Fig. 5a, and indeed this is close to the simulation result, $\langle v \rangle_{sat} = \sqrt{3.2}$ from Fig. 6. This means that $\langle v \rangle_{sat}/v_b = 0.89$, namely 11% average slowing down from the initial speed.

This discussion also implies that the closer the input parameter, $k_\perp v_b/\omega_{ci}$, is to that of the Bessel function peak the less will be the net drop in the average speed of beam at the saturation time, thus possibly providing a way of controlling the amount of the collisionless slowing down.

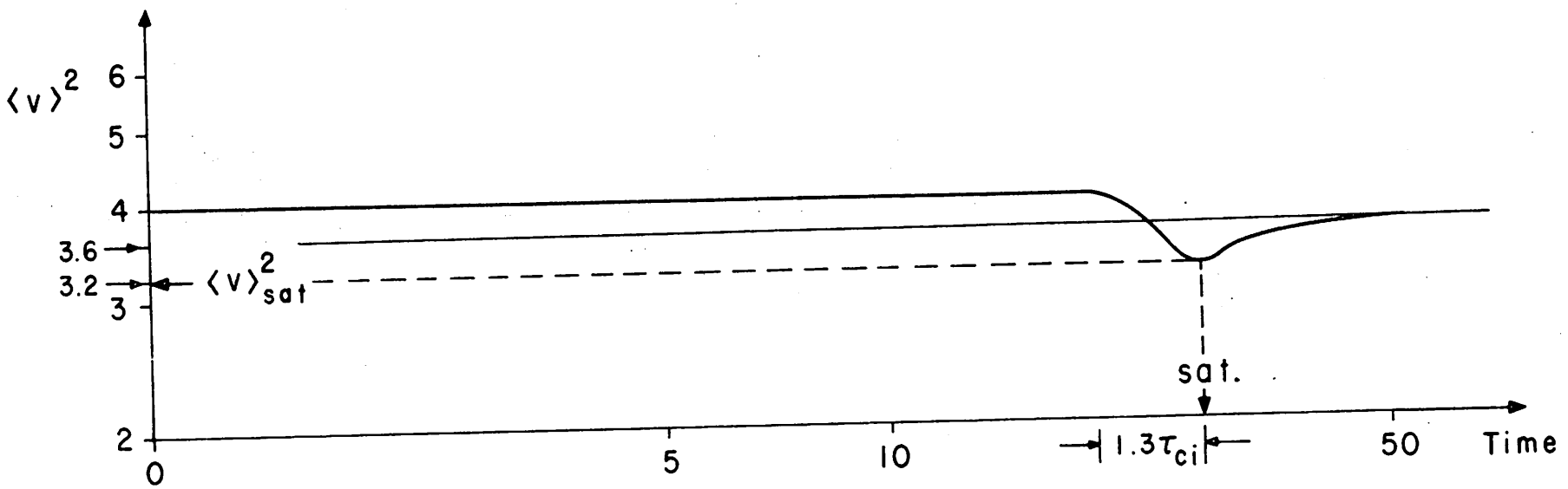

Fig. 6 The time evolution of the square of the average speed of beam particles; it takes about one ion cyclotron period from when a noticeable change appears to when the wave reaches its first peak amplitude (called "saturation").

Changing to a 10 times denser plasma, $\omega_{ppi}/\omega_{ci} \approx 32$ (but still $R = 10^{-2}$), we observe $v_1/v_b = 1.2 - 1.3$ (compared to 1.14 for the $\omega_{ppi}/\omega_{ci} = 10$ case discussed before) and $\langle v \rangle_{sat.}/v_b \approx 0.96$ (compared to 0.89 before); that is, the spreading is much larger, while the slowing is much less.

(3) *Saturation Levels: Simulation Classification and Theoretical Estimations*

Wave growth eventually stops. We define the saturation time and level when the field energy reaches its first peak. It is postulated that saturation occurs by the trapping of ring particles in the perpendicularly propagating wave potential, analogous to the more familiar beam-plasma model.

The evidence that saturation occurs by trapping is as follows. First, the electric field energy in simulation increases exponentially as predicted by the linear theory; then after a stage of a reduced growth rate, it reaches its first maximum value, and drops to its first minimum, and then oscillates with a frequency close to the trapping frequency of the dominant mode. These oscillations are observed in the simulations for all three ring density regimes. Similar oscillation is observed in the ring mean speed with phase opposite to that of the field energy (part of it was shown in Fig. 6). Secondly, the phase space plots (v_x vs x) and the perpendicular velocity space plots (v_x vs v_y like Fig. 2) show vortex-like structures in the particles, indicative of trapping, as the instability becomes large in amplitude.

Saturation by another mechanism, e.g., quasilinear diffusion, was considered by Kulygin *et al.* (1971), Seiler *et al.* (1976, 1977), and Yamada *et al.* (1977). In our simulations, however, quasilinear saturation would be difficult to observe because (i) the mode density in the vicinity of the fastest growing wave was small, and (ii) the ring

in our simulations had no initial thermal spread, allowing only a small spread in allowable phase velocities.

Simulations provide extensive information about the saturation phenomenon, summarized in Fig. 7, where we observe that the classification via the saturation levels of simulations (η, the ratio of the first maximum of electric field energy to the initial beam kinetic energy) is closely related to that via the maximum growth rates (see Fig. 2 of the previous paper, Part I). The two sets of simulation results in the weak regime (i.e., $R \lesssim 5 \times 10^{-3}$) show the effect of the mode structure in simulations, namely, whether the theoretically most unstable mode is allowed in a simulation or not; this effect is especially important where there is discrete mode structure as in the weak ring cases. The effect also occurs in an unmagnetized beam-plasma instability simulation, where the saturation level is greatly affected whether the theoretically most unstable mode is allowed in the simulation, with a finite number of modes excited [Lee and Birdsall (1978)].

In the following we present a way of estimating the saturation levels (η) analytically with their comparison with simulation results.

From energy conservation, the initial (noted by a superscript o) kinetic energy of the beam KE_b^o supplies the kinetic energy change of the plasma and the electrostatic energy at saturation (noted by a prime) as

$$KE_b^o = KE_b' + \delta KE_p' + ESE' \qquad (2)$$

This statement readily is rearranged to read as

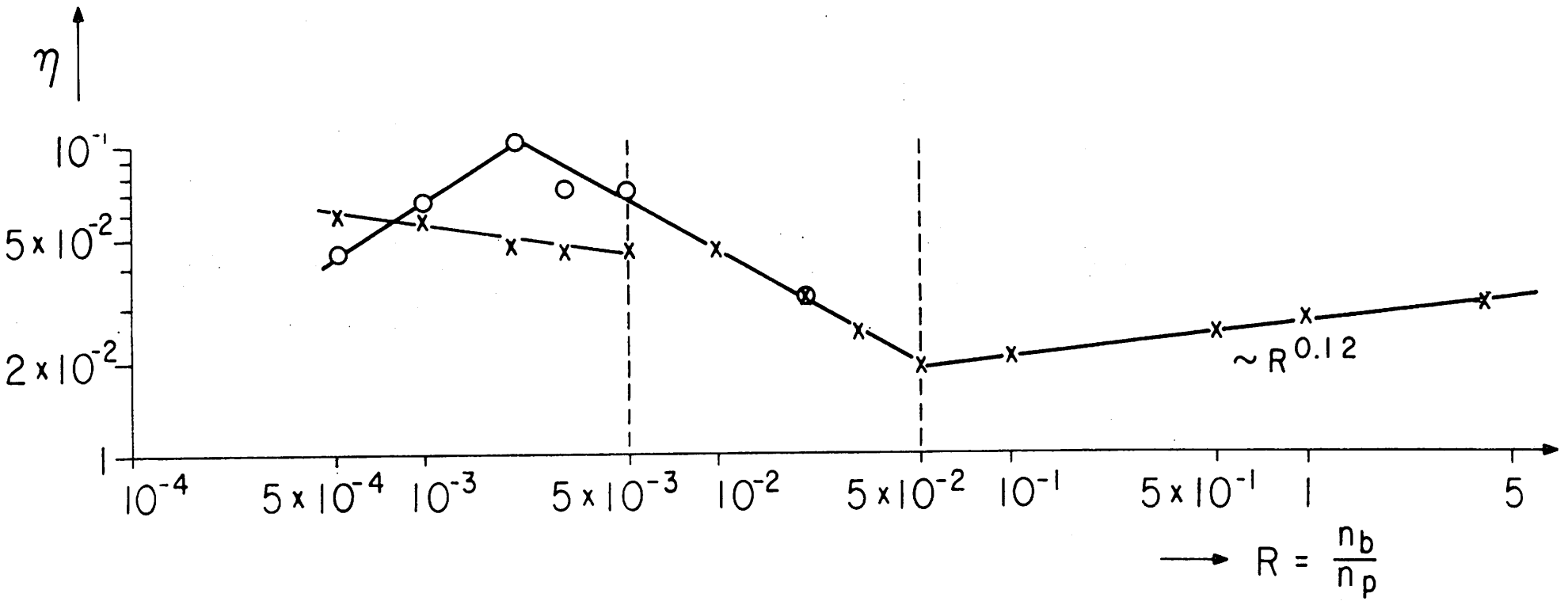

Fig. 7 Saturation levels (η) in electrostatic simulations with the same parameters as in Fig. 2 of Part I. The two sets of results in the weak regime correspond to two different simulations with and without the theoretically most unstable mode included (marked 0 and x, respectively); these two different simulations provide identical values in the intermediate or strong regimes. Straight lines are drawn just to connect these simulation points.

$$1 = \frac{KE_b'}{KE_b^o} + \frac{\delta KE_p'}{KE_b^o} + \eta \tag{3}$$

We make the following approximations. First, the ratio of the kinetic energy of plasma sloshing in the wave trough to the field energy is [Krall and Trivelpiece (1973)]

$$\frac{1}{\eta} \frac{\delta KE_p'}{KE_b^o} \approx \omega \frac{\delta \varepsilon_p}{\partial \omega}\bigg|_\omega - 1 \tag{4}$$

Here, the dielectric constant of the fluid plasma is approximately that of an unmagnetized one since the wave frequency is much larger than the cyclotron frequency, i.e.,

$$\varepsilon_p \approx 1 - \frac{\omega_{ppi}^2}{\omega^2} \left(1 + 3 \frac{k_\perp^2 v_{tp}^2}{2\omega^2}\right)$$

Thus, for the same parameters as in simulations in the weak or intermediate ring regime, the above formula predicts

$$\frac{1}{\eta} \frac{\delta KE_p'}{KE_b^o} \approx 1.05 \tag{5}$$

This value was checked with simulation results within 3% for $5 \times 10^{-4} \leq R \leq 3 \times 10^{-2}$. Our second approximation is

$$\frac{KE_b'}{KE_b^o} = \frac{(v^2)_{saturation}}{v_b^2} \approx \frac{\langle v \rangle^2_{saturation}}{v_b^2} \tag{6}$$

where $\langle v \rangle_{sat.}$ is obtained approximately from the argument $x = \frac{k_\perp \langle v \rangle_{sat.}}{\omega_{ci}}$ which makes the corresonding Bessel function $J_\ell(x)$ peaked (cf. Fig. 5). The index ℓ corresponds to the integer closest to $\omega_{real}/\omega_{ci}$. Combining Eqs. (2-6), we obtain order of magnitude estimations for η mostly in the weak ring regime, summarized in Table 1. The comparison with simulation results is only qualitative; considering, however, all the approximations leading to this estimation, we find it rather satisfactory.

$R = n_b/n_p$		5×10^{-4}	10^{-3}	2×10^{-3}	3×10^{-3}	5×10^{-3}	2×10^{-2}
Type A	Simulation	4.7%	6.9%	9.7%	6.8%	7.0%	3.2%
	Estimation	3.8%	4.6%	5.2%	7.0%	2.9%	5.4%
Type B	Simulation	6.0%	5.9%	4.8%	4.6%	4.5%	3.2%
	Estimation	3.8%	1.9%	1.9%	4.5%	4.5%	7.0%

Table 1.

Comparison of saturation levels (η) of electrostatic simulations and theoretical estimations. Types (A) and (B) correspond to that with and without the theoretically most unstable mode included as in Fig. 7.

V. ELECTROMAGNETIC SIMULATIONS

To simulate an electromagnetic ring-plasma instability, we need to use a new hybrid code; its construction is similar to that of an electrostatic hybrid version described in Sec. II. For an electromagnetic version, we combined an electromagnetic particle code, EM1 [Langdon (1970), Cohen *et al.* (1975)] with an electromagnetic Eulerian fluid linearized code, EFL [Lee and Birdsall (1978)].

The verification of the electromagnetic linear Vlasov theory described in Part I with this electromagnetic hybrid code (EM1 + EFL) was quite successful. Some typical results in the linear regime are presented in Figs. 8-10, which show as remarkable agreement as in the previous electrostatic hybrid simulations. Only three modes are available in the wave vector ranges of Figs. 8-9 due to the restrictive parameters of electromagnetic simulations; among these three, the first modes were not observed to grow in the present simulations, but this check could be done with more care in simulations.

The nonlinear evolution of electromagnetic simulations shows a similar pattern to that of electrostatic simulations; namely, the ring particles spread and slow down as nonlinear effects saturate the instability (again by trapping). The quantitative check with analytic explanations as in electrostatic simulations (Sec. IV) has not been attempted yet.

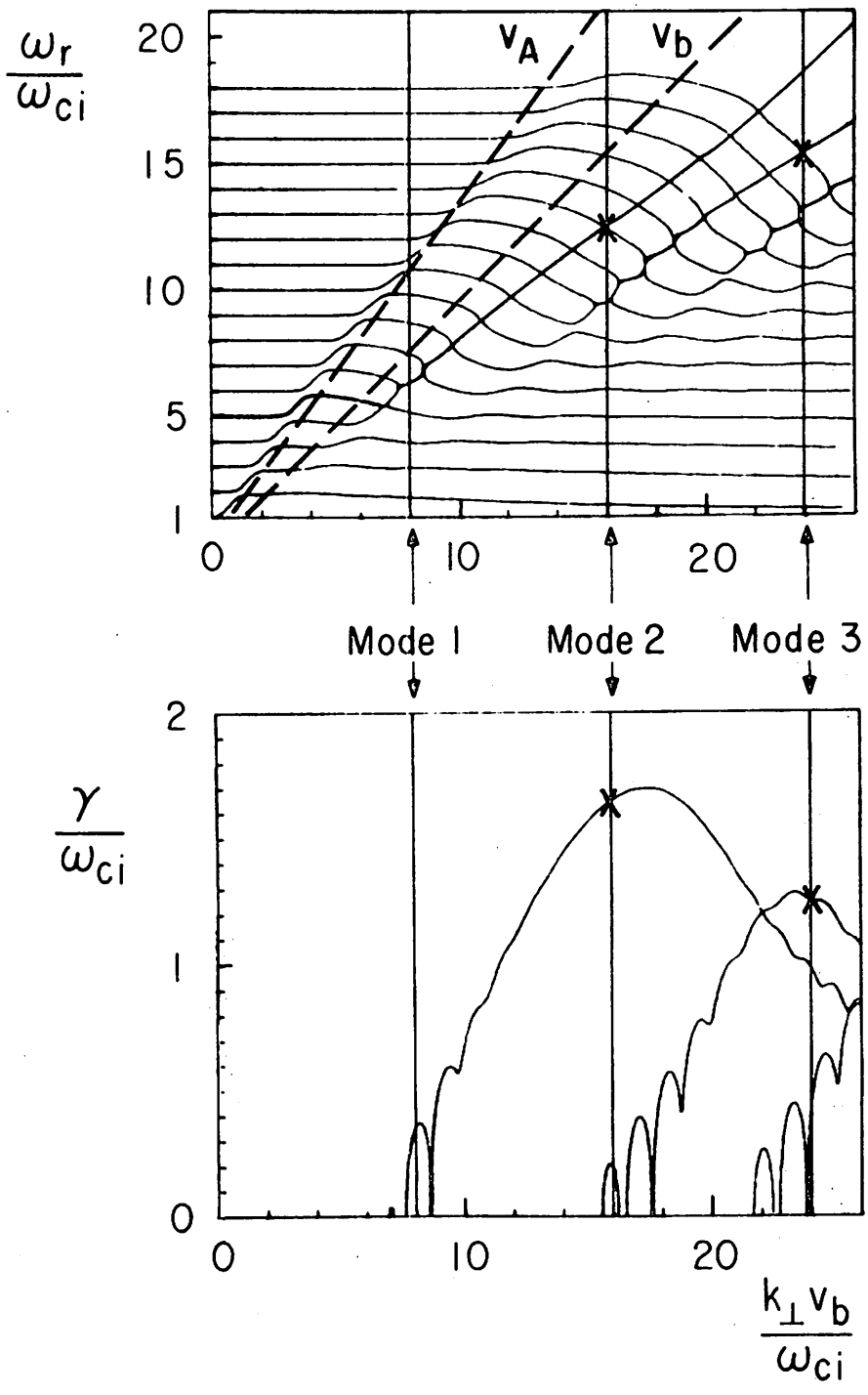

Fig. 8 Electromagnetic hybrid simulation results (marked x) for $R = 0.1$, $\omega_{ppi}/\omega_{ci} \approx 32$, $v_b/v_{tp} \approx 13$, $v_b/v_A \approx 0.9$ (v_A is the Alfven speed), $m_i/m_e = 400$; mode 2 and 3 are almost exactly checked with the theoretical predictions (curves).

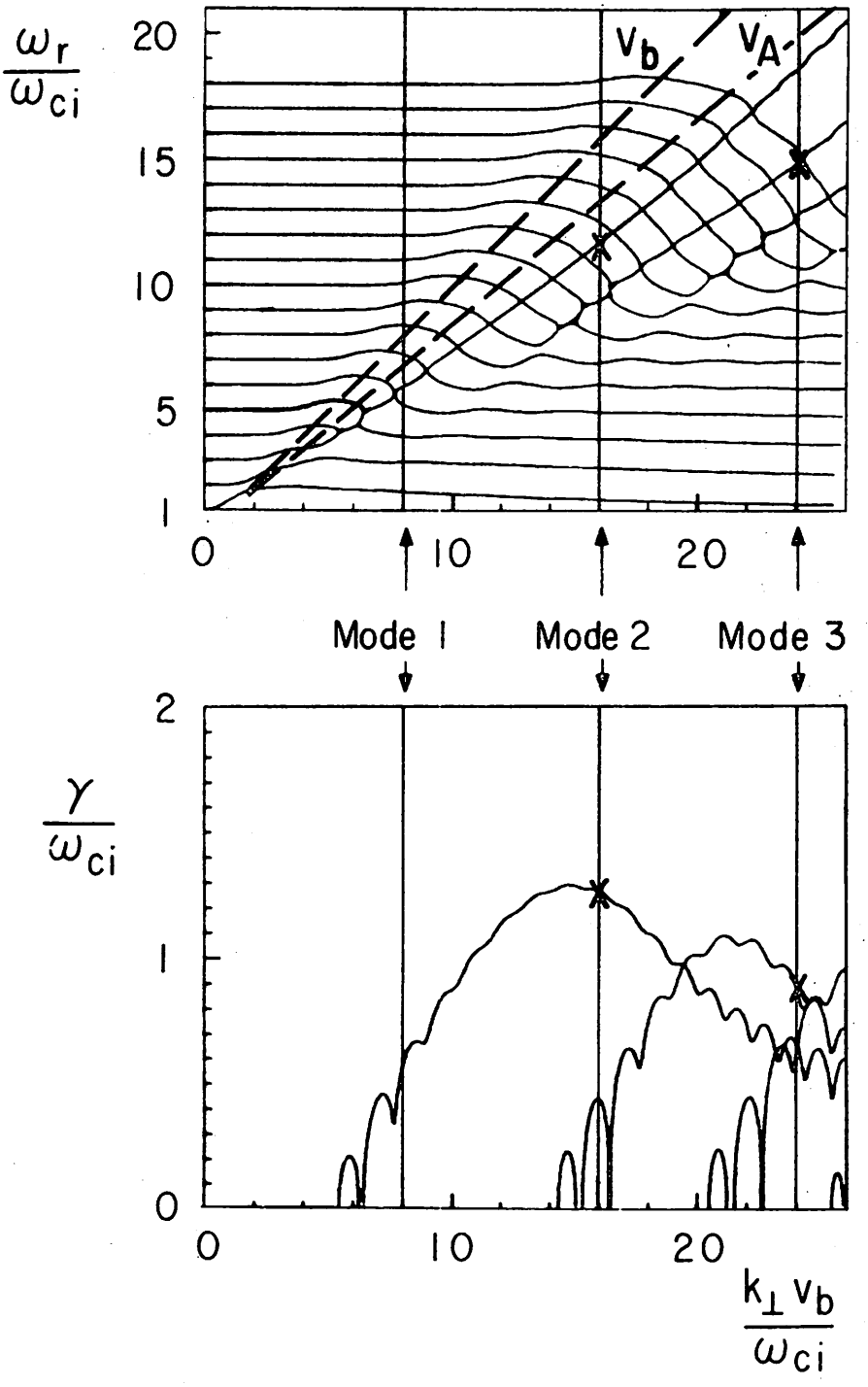

Fig. 9 Same case as in Fig. 8 except for more electromagnetic effects, namely, $v_b/b_A = 1.1$.

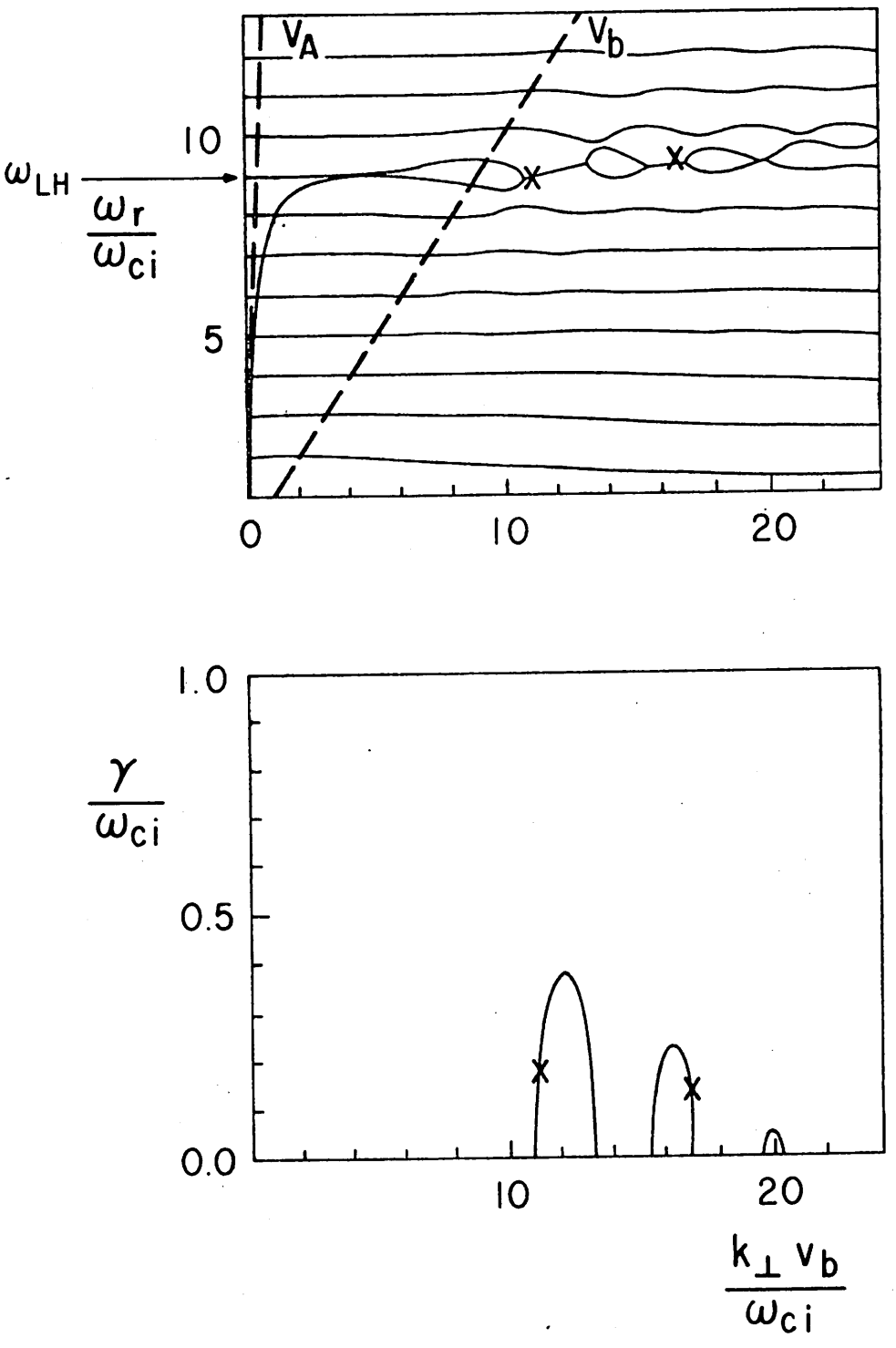

Fig. 10 Electromagnetic hybrid simulation (marked x for the only two growing modes in this wave vector range) with $R = 10^{-2}$, $\omega_{ppi}/\omega_{ci} = 10$, $v_b/v_{tp} \approx 13$, $v_b/v_A = 0.07$ (only slightly electromagnetic).

VI. LIMITS on THE LINEARITY ASSUMPTION of THE FLUID PLASMA

The linearity assumption is good only when perturbed fluid plasma velocities (v_1) remain small compared to the wave phase velocity (ω/k).

We find that this criterion is satisfied for weak or intermediate beam regimes but not for the strong beam regime at saturation. In Fig. 11, the maximum perturbed plasma velocity is seen to be not negligibly small, especially near and after the saturation, at large ring strength. In order to allow larger nonlinearity in the fluid plasma, changing to a new model (e.g., using a Lagrangian fluid) is recommended.

However, for this strong beam regime, saturation levels (η) show that the power dependence of η on the ring strength (R) is

$$\eta \sim R^{0.12} \qquad \text{(from Fig. 7)}$$

while

$$\frac{\gamma_{max}}{\omega} \sim R^{0.17} \qquad \text{(from Fig. 2 of Part I)}$$

The 0.12 value observed is close to the value of 0.17; this is contrasted to the $\underline{B}_o = 0$ beam-plasma case, where the R-dependences of η and γ_{max} are the same [Drummond et al. (1970)]. Thus, the simulation saturation levels (although dubious due to the breakdown of the linearization) might still contain some measure of credibility even for strong beam cases.

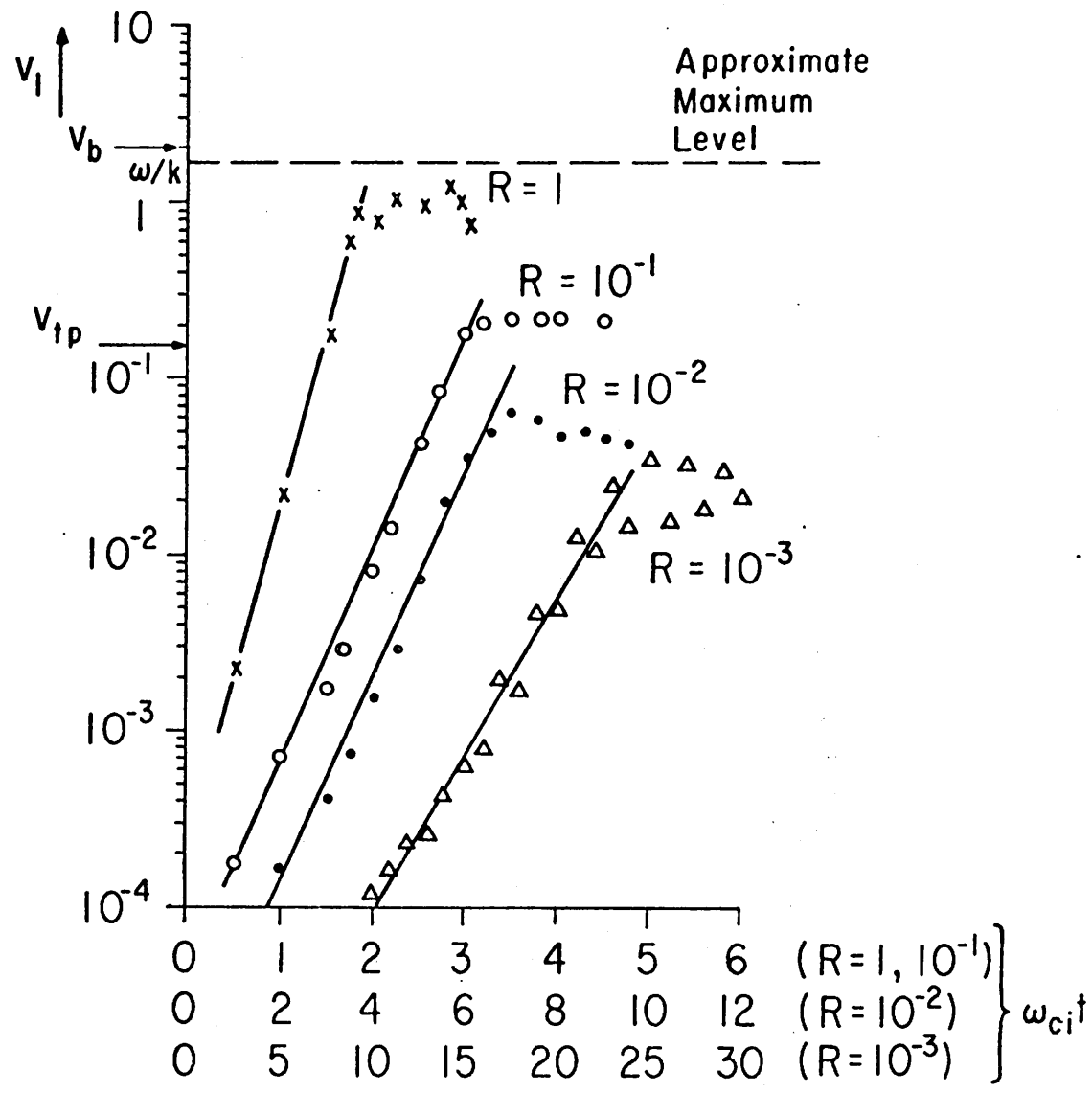

Fig. 11 The time evolution of the maximum perturbed plasma fluid velocities (v_l) for R=1 , 10^{-1} , 10^{-2} and 10^{-3} , obtained from electrostatic hybrid simulations with $\omega_{ppi}/\omega_{ci} \approx 32$, $v_b/v_{tp} \approx 13$, $v_A/v_b = \infty$. Note that the linearity assumption does not hold near the saturation time espectially for strong beams where the wave phase velocity (ω/k) is about 1.6 close to the perturbed velocities.

VII. CONTRAST BETWEEN WHOLLY PARTICLE-THEORY and FLUID-PARTICLE THEORY

In hybrid simulations the ring component is treated as particles and the plasma component as a fluid, thus providing only ring Bernstein harmonics with no plasma Bernstein harmonics. Simulation results using fluid and particles for the two components agree very closely with the theoretical predictions using Vlasov models both for the ring and for the plasma. This agreement is expected in accordance with the argument by Cary and Kaufman (1977) because the discrepancy between the Vlasov theory and the fluid theory vanishes at zero electron thermal spread, which indeed is our case. This gives us further evidence (in addition to that in Sec IV(5) of Part I) to the conclusion that when the lower hybrid coupling occurs (as at $R \ll 1$) it couples with ring Bernstein harmonics rather than with plasma Bernstein harmonics for a cold ring case. With larger ring thermal spread than used here, however, this coupling may change from the previous fluid type to the resonant kinetic coupling, in which the frequency mismatch is an important factor and plasma Bernstein harmonics may play a role as in the case studied experimentally by Seiler *et al.* (1976), Seiler (1977), and Yamada *et al.* (1977).

VIII. CONCLUSIONS

In the preceding paper, Part I and in this Part II, we studied a flute-like velocity-space instability, arising from the large difference in the ion velocity distributions (perpendicular to a uniform magnetic field) of a homogeneous two-energy component plasma. In Part I, the linear Vlasov theory (electrostatic and electromagnetic) was used, and in Part II, computer simulations were used.

Simulations using particle-fluid hybrid codes show remarkable agreement with the linear Vlasov theory both in electrostatic and in electromagnetic cases for a wide range of ring density relative to plasma density.

Hybrid simulations also reveal interesting nonlinear (large amplitude) evolution. At the end of linear growth (saturation) there is appreciable spreading ($\sim$10% each outward and inward in the $v_\perp$ space), and slowing down ($\sim$10%) of the initially monoenergetic beam particles, and saturation occurs by trapping. These effects all occur on a faster time scale ($\sim$ a few ion cyclotron periods) than the collision-caused relaxation phenomena which may now be followed requiring Fokker Planck-like solutions. Some of these simulation nonlinear features agree well with analytic explanations.

Electromagnetic effects tend to reduce the instability growth rate as the Alfven speed is made closer to or smaller than the beam perpendicular speed, namely in a very high beta plasma.

The use of a linearized fluid for the plasma component was justified except when the beam is very strong and the instability is near the saturation stage.

ACKNOWLEDGMENTS

We are very grateful to William M. Nevins for his tireless discussions and help, and A. Bruce Langdon for suggesting the use of a hybrid simulation for this instability study. We also acknowledge the benefits from the discussions with Yoshi Matsuda and Gary Smith.

This work was supported by the U.S. Department of Energy Contract EY-76-S-03-0034-PA128.

REFERENCES

1969 Aamodt, R. E. and Bodner, S. E., "Nonlinear Dynamics of a Single Harmonic Loss-Cone Flute Mode", Phys. Fluids 12, pp. 1471-1480, July.

1970 Aamodt, R. E., "Nonlinear Evolution of Multiple-Finite Amplitude Resonant Loss-Cone Modes", Phys. Fluids 13, pp. 2147-2161, August.

Drummond, W. E., Malmberg, J. H., O'Neil, T. M. and Thompson, J. R., "Nonlinear Development of the Beam-Plasma Instability," Phys. Fluids 13, pp. 2422-2424, August.

Langdon, A. B., "Investigations of a Sheet Model for a Bounded Plasma with Magnetic Field and Radiation," Ph.D. Thesis, Princeton University.

1971 Kulygin, V.M., Mikhailovskii, A. B. and Tsapelkin, E. S., "Quasi-linear Relaxation of Fast Ions Moving Transverse to a Magnetic Field", Plasma Phys. 13, pp. 1111-1116, December.

1973 Krall, N. A. and Trivelpiece, A. W., Principles of Plasma Physics, p. 139, McGraw-Hill Book Co.

1974 Timofeev, A. V., "Confinement of Charged Particles in Adiabatic Traps in the Presence of Monochromatic Cyclotron Oscillations", Nuclear Fusion 14, pp. 165-171.

1975 Cohen, B. I., Mostrom, M. A., Nicholson, D.R., Kaufman, A. N. and Max, C. E., "Simulation of Laser Beat Heating of a Plasma", Phys. Fluids 18, pp. 470-474, April.

1976 Birdsall, C. K., Gerver, M. J. and Maron, N., "Ring-Plasma Instability: Theory and Simulation", Bull. Am. Phys. Soc. 21, p. 1148, October.

Gerver, M. J., Memorandum No. M77/27, Oct. 31 (University of California; Electronics Research Laboratory).

Seiler, S., Yamada, M. and Ikezi, H., "Lower Hybrid Instability Driven by a Spiraling Ion Beam", Phys. Rev. Lett. 37, pp. 700-703, September.

1977 Cary, J. R. and Kaufman, A. N., "Quasistatic Magnetic Field Generation by a Langmuir Wave Packet", Bull. Am. Phys. Soc. 22, p. 1103, October; the details leading to the conclusion cited in our paper can be found in Cary's forthcoming thesis, University of California, Berkeley.

Fukuyama, A., Momota, H., Itatani, R. and Takizuka, T., "Stochastic Acceleration by an Electrostatic Wave near Ion Cyclotron Harmonics", Phys. Rev. Lett. 38, pp. 701-704, March.

Lee, J. K. and Birdsall, C. K., "Ring-Plasma Instability, Linear Theory, Simulation, Nonlinear Behavior", Bull. Am. Phys. Soc. 22, p. 1109, October.

Seiler, S., "Linear and Nonlinear Development of a Lower-Hybrid Wave Driven by a Perpendicular Ion Beam," Ph.D. Thesis, Princeton University.

Yamada, M. and Seiler, S., "Anomalous Slowing of a Perpendicularly Injected Ion Beam in Both Quasilinear and Trapping Regimes", Phys. Rev. Lett. 39, pp. 808-811, September.

1978 Lee, J. K. and Birdsall, C. K., "Particle-Fluid Simulations Applied to Beam-Plasma and Ring-Plasma Instabilities", Proc. of the Eighth Conf. on Numerical Simulation of Plasmas, PC-10; with an addition, to be submitted to Jour. of Comp. Phys.